Microwave-assisted synthesis of highly dispersed ZrO2 on CNTs as an efficient catalyst for producing 5-hydroxymethylfurfural (5-HMF)

DOI:
10.1016/j.fuproc.2022.107292

Document Version
Final published version

Fuel Processing Technology 233 (2022) 107292

Contents lists available at ScienceDirect

Fuel Processing Technology

journal homepage: www.elsevier.com/locate/fuproc

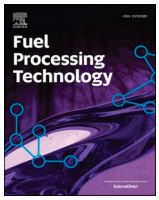

Microwave-assisted synthesis of highly dispersed ZrO_2 on CNTs as an efficient catalyst for producing 5-hydroxymethylfurfural (5-HMF)

Shiyun Mu [a,1], Kai Liu [a,1], Hong Li [a,1], Zhenyu Zhao [a], Xiaoqi Lyu [a], Yilai Jiao [c,*], Xingang Li [a,b], Xin Gao [a,b,**], Xiaolei Fan [d]

[a] School of Chemical Engineering and Technology, National Engineering Research Center of Distillation Technology, Collaborative Innovation Center of Chemical Science and Engineering (Tianjin), Tianjin University, Tianjin 300072, China
[b] Haihe Laboratory of Sustainable Chemical Transformations, Tianjin 300192, China
[c] Institute of Metal Research, Chinese Academy of Sciences, 72 Wenhua Road, Shenyang 110016, China
[d] Department of Chemical Engineering, School of Engineering, The University of Manchester, Oxford Road, Manchester M13 9PL, United Kingdom

ARTICLE INFO

Keywords:
Microwave (MW)
Multi-walled carbon nanotubes (MWCNTs)
Zirconia
Fructose dehydration
5-Hydroxymethylfurfural (5-HMF)

ABSTRACT

This work presents an efficient method of supporting zirconia (ZrO_2) on —COOH functionalized multi-walled carbon nanotubes (ZrO_2/MWCNTs(C)) via a microwave (MW)-assisted method, which can be used as an efficient catalyst for converting fructose to 5-HMF. The developed composite by the MW-assisted route shows highly dispersed ZrO_2 with small sizes of 4–5 nm on the carbon support, which could not be achieved the conventional hydrothermal synthesis. Characterization shows a unique zirconia amorphous structure which was ascribed to the special interaction between the carbon support and MW irradiation. Specifically, MWCNTs were heated selectively due to their strong MW-absorbing ability, which led to the formation of microscopic "hot spots", enabling rapid synthesis (8 min) of highly dispersed ZrO_2 with smaller sizes on the hot surface of MWCNTs. Conversely, under conventional heating, the nucleation rate of ZrO_2 was slow and prone to form agglomerated particles on the carbon support. The amorphous ZrO_2 contributed to the excellent activity of ZrO_2/MWCNTs(C) in fructose conversion to 5-HMF. In detail, fructose conversion and 5-HMF yield were achieved at ~72.8% and ~62.9%, respectively, for the catalyst prepared by the MW method, whilst they are only about 24.7% and 15.7% over the catalyst prepared by the conventional hydrothermal synthesis.

1. Introduction

Currently, the demand for green and renewable energy increases significantly due to the call of sustainable development [1,2]. Biomass is an important resource for developing sustainable energy, fuels and chemicals [3]. Nowadays, utilization of biomass is focused mainly on biofuels such ethanol [4], biodiesel [5] and biogas [6], as well as various platform compounds to replace ones from fossil fuels in the production of chemicals [7]. Among the bio-based chemicals, 5-hydroxymethylfurfural (5-HMF) is regarded as an important platform molecule to be derived to various value-added chemicals (such as furan derivatives, succinic acid, and liquid alkanes) [8]. Currently, catalytic hydrolysis of sugars is the common approach to prepare 5-HMF [9], thus, the development of advanced catalysts is critical to progress efficient production processes for preparing 5-HMF.

Due to its excellent mechanical properties, great chemical/thermal stability, and functional acidic/basic properties [10], zirconium oxide (or zirconia, ZrO_2) is a perfect catalyst for various reactions, such as methane decomposition [11], water gas shift [12], and biomass dehydration [13]. Moreover, recent studies found that the particle size of ZrO_2 played a vital role in its catalytic activity [14–16]. For example, Liu et al. [14] found that a decrease in the particle size of the supported ZrO_2 on MWCNTs (from 9 to 2 nm) increased the contact area between the catalyst and solutions containing substrates, thus enhancing catalytic activity in biomass conversion reaction. In addition, the catalyst support would also have a significant influence on the particle size and

* Correspondence to: Yilai Jiao, Institute of Metal Research, Chinese Academy of Sciences, 72 Wenhua Road, Shenyang 110016, China.
** Correspondence to: Xin Gao, School of Chemical Engineering and Technology, National Engineering Research Center of Distillation Technology, Collaborative Innovation Center of Chemical Science and Engineering (Tianjin), Tianjin University, Tianjin 300072, China.
E-mail addresses: yljiao@imr.ac.cn (Y. Jiao), gaoxin@tju.edu.cn (X. Gao).
[1] These authors contributed equally.

https://doi.org/10.1016/j.fuproc.2022.107292
Received 20 February 2022; Received in revised form 5 April 2022; Accepted 16 April 2022

dispersion of the supported ZrO_2, which affects the performance of the catalyst. For instance, Li et al. [17] synthesized ZrO_2/SBA-15 catalysts using the mesoporous SBA-15 with high specific surface area (600–1000 $m^2 \cdot g^{-1}$) as support, and the mesoporous structure of SBA-15 enabled ZrO_2 to be uniformly dispersed on the surface of the support to form a monodisperse ZrO_2 phase with the particle size of <10 nm. The uniform dispersion and small particles promoted the exposure of the active sites on ZrO_2, extremely improving the catalytic activity of the catalyst. In detail, ~92.6% conversion was achieved by using the supported ZrO_2 in the esterification reaction of pyrolysis oil, which was much higher than that of the conventional bulk ZrO_2 catalyst.

Due to the large specific area and excellent chemical and physical stability, carbon nanotubes (CNTs), such as multi-walled (MWCNTs) and single-walled (SWCNTs) are widely used as the catalyst supports for preparing supported catalysts [18,19]. Especially in hydrothermal synthesis, with the aim to make the ZrO_2 particles more uniformly distributed on the surface of CNTs and prevent particle aggregation, surface modification is usually required to increase the number of functional groups (such as —COOH, —OH, and —C═O) on the surface of CNTs, which can act as nucleation sites for anchoring ZrO_2 [20–23]. For example, Liu et al. [14,24] used nitric acid to functionalize the surface of MWCNTs and introduced a large number of oxygen-containing functional groups (—COOH, —OH, and —C═O) on the surface of MWCNTs, facilitating uniform growth of ZrO_2 particles on MWCNTs. Besides, the C K-edge NEXAFS characterization showed that the oxygen-containing groups on MWCNT interact with Zr precursor during the hydrothermal synthesis (at 180 °C and 20 atm for 6 h) to form a strong C—O—Zr bond between ZrO_2 and MWCNTs, improving the stability of the supported ZrO_2 catalyst on MWCNTs. In contrast, ZrO_2 was prone to agglomerate on the surface in the hydrothermal synthesis with unacidified MWCNTs as catalyst support. Notably, although previous studies have demonstrated the effectiveness of using versatile CNTs to control the size of supported zirconia, the current hydrothermal methods for preparing the zirconia nanoparticles-CNTs composite catalyst are rather harsh, time- and energy-consuming.

Compared to the classic contact heating that relies on heat conduction and convection, microwave (MW)-induced heating has its unique advantage, such as high heating efficiency, selectively heating, and microwave-induced "hot spot" effect [25]. With the mentioned advantages, microwave irradiation has become a means of process intensification in material synthesis and chemical reactions [26]. For example, MW irradiation could accelerate the synthesis of MIL-88 significantly, reducing the synthetic time from several days required in conventional hydrothermal synthesis to several minutes [27]. Similarly, benefiting from the rapid heating, the particle size of MIL-88 synthesized by MW-assisted method (about 0.2 μm) is smaller than that of conventional hydrothermal method (>2 μm). Furthermore, the MW-assisted synthesis can be further enhanced when the MW-absorbing material is used to form "hot spot" [28]. In previous work, the highly MW-absorbing SiC was preferentially heated by MW, which enabled the selective growth of uniform ZSM-5 on the SiC surface and suppressed the formation of ZSM-5 crystals in the liquid phase [29]. Particularly, carbon materials (including CNTs) are considered as excellent microwave absorbers due to their large dielectric constants (ranging from 3 to 16) [30,31]. Therefore, accordingly, when considering the preparation of supported ZrO_2 on CNTs, MW-assisted synthesis would be a rational choice to intensify the synthesis and control the property of the supported ZrO_2.

Herein, in this paper, we used the MW-hydrothermal method to synthesize highly dispersed nano-zirconia-loaded ZrO_2/MWCNTs composite catalysts with tiny particle diameters through the "hot spot" effect to provide a powerful catalyst for the catalytic conversion of fructose to 5-HMF. According to conventional hydrothermal synthesis methods, carboxyl groups on the surface of CNTs are necessary to provide nucleation sites for anchoring ZrO_2 on CNTs [32]. Therefore, the MWCNTs with carboxyl groups were used in this work. Meanwhile, the structures of catalysts were characterized and compared with catalysts from conventional hydrothermal synthesis, in order to further reveal the mechanism of MW-hydrothermal synthesis and provide a paradigm for understanding the application of MW induced "hot spots" in the synthesis of catalysts. Finally, the model reaction of selective catalytic dehydration of fructose to 5-hydroxymethylfurfural (5-HMF) was used to evaluate the catalytic activity of the developed ZrO_2/MWCNTs composite catalysts.

2. Experimental

2.1. Materials and chemicals

—COOH functionalized MWCNTs (MWCNTs(C), average diameter of 8–15 nm, length of 3–12 μm, purity ≥98 wt%, carboxyl content at about 0.5 $mmol \cdot g^{-1}$) was used in this work as the carbon support to prepare the ZrO_2/MWCNTs composites. $ZrOCl_2 \cdot 8H_2O$ (99 wt%) purchased from Aladdin Reagent Co. Ltd. (Shanghai, China) was used as the Zr precursor for the synthesis. Surfactant polyvinyl pyrrolidonePoly (PVP, average molecular 58,000) supplied by Macklin Biochemical Co., Ltd. (Shanghai, China) was used to improve the dispersibility of carbon nanotubes in solution.

In the activity test of catalysis, chemicals including fructose (≥99 wt %), 5-hydroxymethyl-2-furfural (5-HMF, 99 wt%),and levulinic acid (LA, 99 wt%) were purchased from Aladdin Reagent Co. Ltd. (Shanghai, China). Dimethyl silicone oil (500 cSt, 25 °C as the heat transfer fluid) and dimethyl sulfoxide (DMSO, ≥99.80 wt% as the solvent) were purchased from Heowns Biochemical Technology Co., Ltd. (Tianjin, China).

2.2. Synthesis of ZrO_2/MWCNTs(C) composites

A typical procedure for preparing the supported ZrO_2 on carbon materials under MW irradiation is described below (using MWCNTs(C) as the carbon support). Firstly, MWCNTs(C) powder (0.3 g) was dispersed in 60 mL deionized water with PVP via and ultrasonic treatment for 120 min at room temperature to homogenize the system. Then $ZrOCl_2 \cdot 8H_2O$ (1.176 g, corresponding to about 60 wt% loading) was added into the liquid mixture via ultrasonic treatment for another 30 min. Then the black suspension was placed in a multimodal microwave reactor and heated for 8 min (at 700 W, the equipment of the MW synthesis system was shown in Fig. S1). After the synthesis, the system was cooled to room temperature and centrifuged to separate solids in the system. Then the solids were washed several times using ethanol and dried at 70 °C under vacuum for 12 h. The synthetic time was varied in a range of 5–120 min to investigate its effect on the resulting composites. Unsupported bulk ZrO_2 was also synthesized with the same MW procedure. The conventional hydrothermal synthesis method based on the previous work [22] was used to prepare ZrO_2/MWCNTs composites as the control group catalysts. The catalyst for conventional hydrothermal synthesis is synthesized in stainless steel Teflon-lined autoclave reactor (100 mL capacity, at 180 °C for 720 min). For better differentiation, the obtained composites were named as CH/MW-ZrO_2/MWCNTs(C)-α, in which CH and MW represent the conventional and microwave synthesis method, respectively. α refers to the synthesis time (in min), and the bulk ZrO_2 was named as MW-ZrO_2-8.

2.3. Characterization of materials

Comprehensive characterization of the materials under investigation was achieved by a combination of techniques, including X-ray diffraction (XRD), X-ray photoelectron spectroscopy (XPS), thermogravimetric analysis (TGA), differential scanning calorimetry (DSC), transmission electron microscopy (TEM), high-resolution transmission electron microscopy (HRTEM), Fourier transform infrared (FTIR), pyridine adsorption Fourier-transform infrared (Py-IR), nitrogen (N_2) physisorption and inductively coupled plasma optical emission spectrometry (ICP-OES). The details of the characterization techniques are described

in the part one of Supplementary Information (SI). In order to quantify the MW-absorbing ability of materials, the network analyzer (Keysight, ENA 85033C) equipped with a coaxial probe was used to measure the dielectric constant and loss of the carbonaceous materials (at 2.45 GHz) [33].

2.4. Catalytic fructose conversion

Catalytic fructose dehydration to 5-HMF was carried out in a laboratory batch reactor under conventional heating conditions, and the experimental set-up was shown in Fig. S2. In a typical experiment, 0.2 g of catalyst was added into the reactor with 20 mL DMSO and treated by sonication for 5 min to ensure homogenization of the suspension. After that, the mixture was heated to 120 °C, and then 0.5 g of fructose was charged into the reactor to initiate the reaction. The reaction was performed at 120 °C for 5 min. Afterwards, the reactor was rapidly quenched by immersing it into an ice-water bath. Next, the catalyst was separated from reactants by centrifugation. The liquid sample was analyzed by the high-performance liquid chromatography (HPLC, LC-20AT, Shimadzu, Japan), which was equipped with a refractive index detector (RID-10A, Shimadzu, Japan) and an Aminex HPX-87H column (Bio-Rad). Typically, 5 mM aqueous sulfuric acid solution was used as the mobile phase and delivered with an HPLC pump at 0.6 mL·min^{-1}. Moreover, the fructose conversion and yield/selectivity of 5-HMF were calculated by Eqs. (S1)–(S3) shown in the part two of SI.

3. Results and discussion

3.1. Material characterization

Generally, the conventional hydrothermal synthesis with CNTs as the support requires a reaction at 180 °C for 12 h to obtain ZrO_2/CNTs composite catalysts [34]. In this work, zirconia structure was grown on the surface of MWCNTs(C) successfully regardless of MW or CH hydrothermal conditions. Under the MW conditions, as shown in Fig.S3, a perfect ZrO_2/MWCNTs composite catalyst can be prepared in only 8 min, and the particle size of zirconia on MWCNTs gradually increases with the synthetic time. Comprehensive XRD and FTIR characterization of the materials were performed. As shown in Fig. 1a, by comparing MWCNTs(C) support with the physical mixture of zirconia/MWCNTs (C), the broad hump located at 26.1° can be assigned to the (002) reflections of the graphite phase of MWCNTs(C) [35]. The ZrO_2 scattering hump of the catalyst prepared by the MW hydrothermal (MW-ZrO_2/MWCNTs(C)-8) was not obvious compared to that of the catalyst prepared by the conventional hydrothermal synthesis (i.e., CH-ZrO_2/MWCNTs(C)-720), which could be due to the larger ZrO_2 particles formed by conventional hydrothermal method. In the diffraction pattern of CH-ZrO_2/MWCNTs(C)-720, peaks located at 24.4, 28.2°, 31.5°, and 30.2°, 35.1°, 50.3° belong to the monoclinic crystalline ZrO_2 (m-ZrO_2) [36] and tetragonal ZrO_2 (t-ZrO_2) phases [37], respectively, showing that crystalline ZrO_2 was successfully supported on the MWCNTs(C) under conventional hydrothermal synthesis. Conversely, these diffraction peaks of ZrO_2 phases were not identified in MW-ZrO_2/MWCNTs(C)-8, suggesting the presence of highly dispersed ZrO_2 with small particle size on MWCNTs(C). However, it is also worth noting that amorphous ZrO_2 has a broad halo hump at around 20–40° [38–41], which overlaps with that of MWCNTs(C). Comparing the diffraction patterns of the bulk ZrO_2 with MW-ZrO_2-8 shows that the bulk ZrO_2 synthesized by the MW method was amorphous, which suggested that the supported ZrO_2 in the MW-ZrO_2/MWCNTs(C)-8 could be amorphous.

Fig. 1b shows the FTIR spectra of relevant materials under study. The absorption band centered at 3430 cm^{-1} is assigned to the —OH groups stretching vibration from the carbon support [42]. The band at about 400–750 cm^{-1} identified in CH-ZrO_2/MWCNTs(C)-720 is associated with vibration modes of Zr—O [43,44]. In detail, the peak at ~492 cm^{-1} and ~ 755 cm^{-1} can be attributed to the tetragonal and monoclinic phases of ZrO_2, respectively [45]. However, these FTIR peaks related to crystalline ZrO_2 were not detected in MW-ZrO_2/MWCNTs(C)-8. Therefore, the findings by FTIR agree well with that of XRD analysis, suggesting the presence of amorphous ZrO_2 in the composite prepared by the MW synthesis.

In order to further investigate the surface composition of the synthesized materials, XPS measurement was carried out, and the results were presented in Fig. 2. As shown in Fig. 2a, the XPS survey scans of the materials show the presence of elemental peaks of O 1 s, Zr 3 s, Zr 3p, and Zr 3d in the two composites, which confirms the formation of ZrO_2 phases on the surface of MWCNTs(C) after the CH and MW hydrothermal synthesis. By comparing the XPS spectra of CH-ZrO_2/MWCNTs(C)-720 and MWCNTs(C), the Zr 3d peaks appear in CH-ZrO_2/MWCNTs(C)-720 and the peak intensity of C at 284.6 eV in MWCNTs(C) decreases greatly as well as the peak intensity of O increases sharply, suggesting that the MWCNTs(C) was coated by ZrO_2 phase after the MW hydrothermal synthesis [20]. However, the intensity of Zr and O in the XPS spectra of MW-ZrO_2/MWCNTs(C)-8 is significantly weaker than that of CH-ZrO_2/MWCNTs(C)-720, suggesting that the relatively low loading of ZrO_2 in the composites prepared by the MW hydrothermal synthesis.

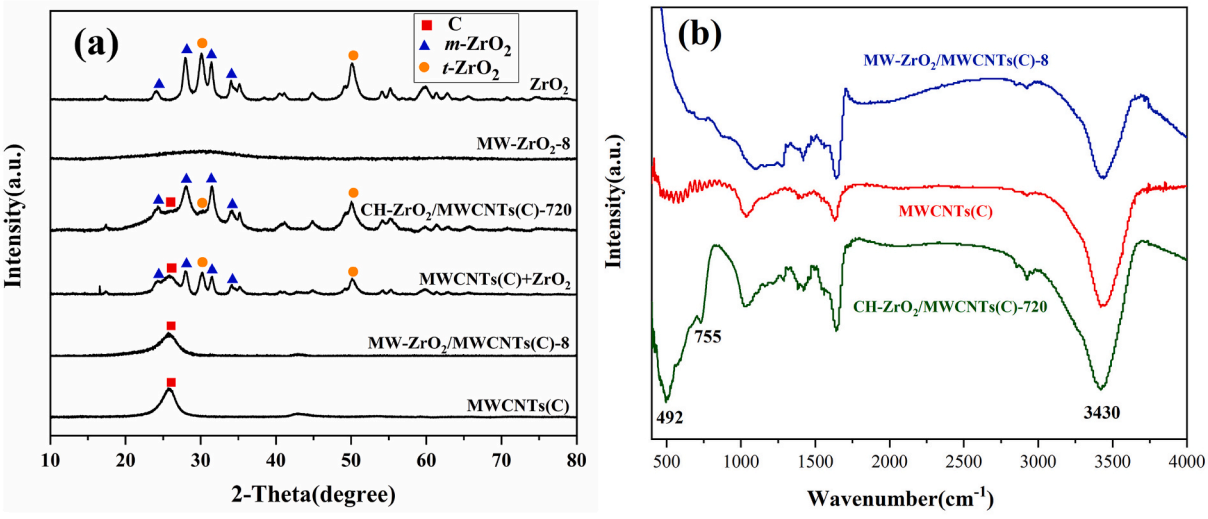

Fig. 1. (a) XRD patterns of ZrO_2/MWCNTs(C) composites, MWCNTs(C), ZrO_2 and MWCNTs(C)/ZrO_2 mixture (MWCNTs(C) + ZrO_2) and (b) FTIR spectra of MWCNTs (C) and ZrO_2/MWCNTs(C) composites prepared under MW and hydrothermal conditions.

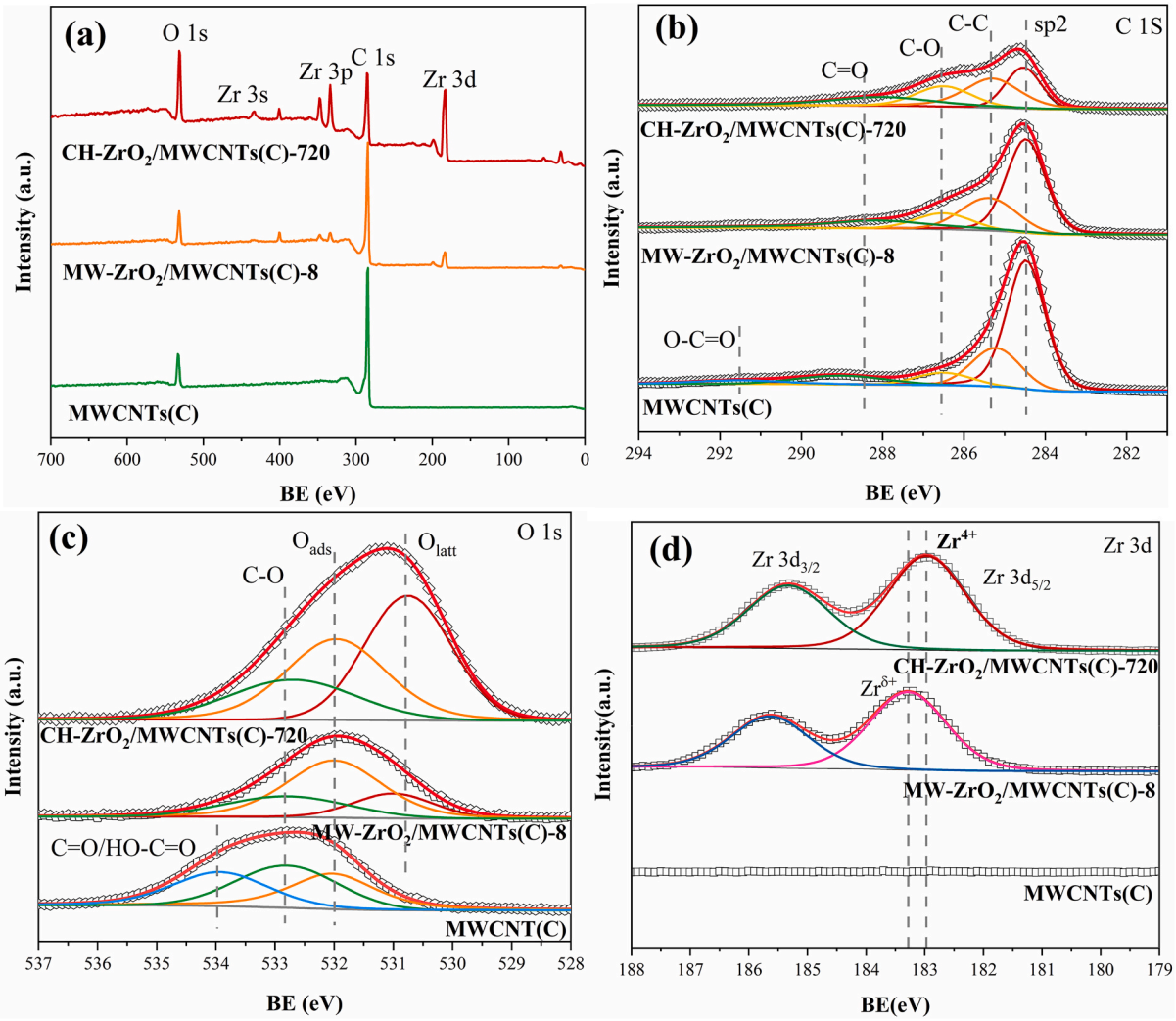

Fig. 2. XPS spectra of MWCNTs(C), MW-ZrO_2/MWCNTs(C)-8 and CH-ZrO_2/MWCNTs(C)-720: (a) survey scan, (b) C 1 s, (c) O 1 s and (d) Zr 3d.

Fig. 2b and c show that the peak protrusions at 291.5 and 533.9 eV represent the carboxyl groups on the MWCNTs(C). Notably, they are less obvious in the spectra of the composites, which implies the possible formation of Zr—O bonds during the synthesis process between Zr precursor and the surface hydroxyl/carboxyl groups of MWCNTs(C). As shown in Fig. 2d, the twin peaks of Zr 3d with the binding energies at 182.9 and 185.3 eV correspond to the Zr $3d_{3/2}$ and Zr $3d_{5/2}$ chemical states, respectively, suggesting the +4 oxidation states Zr and the presence of Zr—O bonds [46]. It also indicates that the zirconia on the support is chemically bonded to the MWCNTs rather than simply physically adsorbed, which can enhance the stability of the composite in catalysis. Ordinarily, ZrO_2 peaks should be located at 182.6 and 185.1 eV. Here, the shift of the ZrO_2 characteristic peak may be due to the electron-withdrawing action of MWCNTs(C) at the binding site [47]. The peaks at 183.2 and 185.9 eV in MW-ZrO_2/MWCNTs(C)-8 can be assigned to $Zr^{\delta+}$, whose binding energy is between Zr^{3+} and Zr^{4+}. Based on the investigation, $Zr^{\delta+}$ corresponds to a new chemical state, in which Zr—O bonds are more covalent than that of ZrO_2 [48]. The formation of the unique Zr structure can be due to the selective heating and "hot spots" formation on MWCNTs(C) under MW irradiation [49,50]. In summary, according to XPS characterization, both the conventional and MW hydrothermal synthesis can prepare the supported ZrO_2 on MWCNTs(C), but the chemical state and loading of the ZrO_2 phases prepared by the two methods are rather different.

The composites (of CH-ZrO_2/MWCNTs(C)-720 and MW-ZrO_2/MWCNTs(C)-8) were further characterized by TEM and HRTEM to understand their physiochemical properties. Fig. 3a–c show that large ZrO_2 particles were formed on MWCNTs(C) of CH-ZrO_2/MWCNTs(C)-720 after the conventional hydrothermal synthesis. Moreover, the ZrO_2 particles on MWCNTs(C) were unevenly distributed and aggregated, which agreed with the previous reports [20]. As shown in Fig. 3d, the particle size distribution (PSD) of the loaded ZrO_2 particles was obtained based on the TEM analysis of the CH-ZrO_2/MWCNTs(C)-720, and the median particle size was about 35 nm. Moreover, the dark-field TEM and EDS mapping of CH-ZrO_2/MWCNTs(C)-720 also show the formation of large ZrO_2 around MWCNTs(C), as shown in Fig. 3e, and it could be due to the preferred nucleation of Zr phases on the surface carboxyl groups on MWCNTs(C). Comparatively, after the 8-min MW synthesis, the resulting supported ZrO_2 particles can hardly be seen in the bright-field TEM images of Fig. 3f and g, as well as in the HRTEM micrograph of Fig. 3h. ZrO_2 particles in MW-ZrO_2/MWCNTs(C)-8 were identified in the Dark-field mode of TEM and EDS, as shown in Fig. 3j, to show the highly and uniformly dispersed ZrO_2 on the surface of MWCNTs(C) with a narrower PSD centered at about 4.5 nm (Fig. 3i). This was further proved by EDS mapping analysis of MW-ZrO_2/MWCNTs(C)-8 (Fig. 3j), in which the presence of Zr, C, and O species with good dispersion on MWCNTs(C) was confirmed, validating that ZrO_2 nanoparticles were grown on MWCNTs(C) successfully after the 8-min MW synthesis. In addition, as shown in Figs. 3h and S5, crystal lattice was not observed for the supported ZrO_2 on MWCNTs(C) under MW synthesis, which

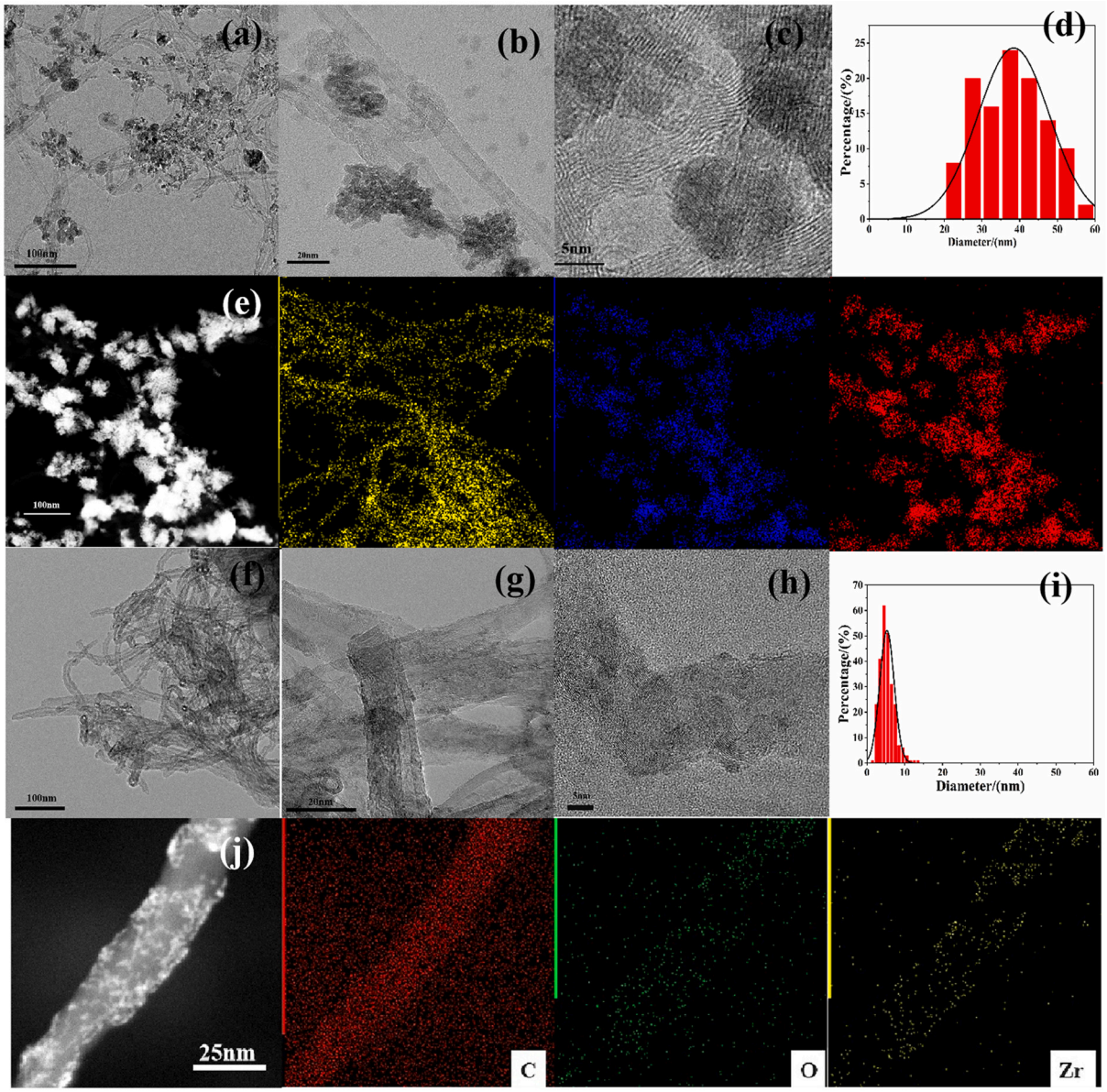

Fig. 3. (a), (b) TEM, (c) HRTEM, (d) particle size distribution (PSD), and (e) EDS mapping of CH-ZrO_2/MWCNTs(C)-720; (f), (g) TEM, (h) HRTEM, (i) PSD, and (j) EDS mapping of MW-ZrO_2/MWCNTs(C)-8.

suggested that amorphous ZrO_2 was prepared by the MW method and in line with the findings by XRD and FTIR.

To conclude, in comparison with the conventional hydrothermal synthesis, the supported ZrO_2 particles synthesized by the MW method have smaller and more uniform particle sizes on the surface of MWCNTs (C). Importantly, in the conventional hydrothermal synthesis, extended synthesis time (e.g. 720 min) was needed to enable the growth of ZrO_2 on MWCNTs(C) with large particles (Fig. S4), while in the MW synthesis, only 8 min was enough for preparing the well-dispersed ZrO_2 nanoparticles on MWCNTs(C). Meanwhile, the supported ZrO_2 prepared by the MW synthesis presents a unique amorphous structure, which is different from the tetragonal and monoclinic ZrO_2 phases prepared by the conventional hydrothermal synthesis. Interestingly, we found that the composite (MW-ZrO_2/MWCNTs-8) can still be synthesized by the MW method even with uncarboxylated MWCNTs, seen in Fig. S6 in SI. A possible explanation is that surface carboxyl groups are no longer necessary to provide nucleation sites for ZrO_2 growth under the MW conditions due to the selective heating of MWCNTs(C), while the high local temperature of the support promotes the growth of ZrO_2 on MWCNTs(C).

TGA and DSC analyses of MWCNTs(C), MW-ZrO_2/MWCNTs(C)-8 and CH-ZrO_2/MWCNTs(C)-720 suggested the nature of the supported ZrO_2 prepared by the two synthesis methods. As shown in Fig. 4, both MW-ZrO_2/MWCNTs(C)-8 and CH-ZrO_2/MWCNTs(C)-720 show the exothermic peak at about 350 °C, and the intensity of the exothermic peaks of CH-ZrO_2/MWCNTs(C)-720 is significantly smaller than that of MW-ZrO_2/MWCNTs(C)-8. According to the literature [39], the exothermic peak at ~350 °C corresponds to the ZrO_2 phase change, transforming from amorphous ZrO_2 to the tetragonal phase. Furthermore, the intensity of the exothermic peak of MW-ZrO_2/MWCNTs(C)-8 at ~350 °C is significantly stronger than that of CH-ZrO_2/MWCNTs(C)-720, indicating that the amorphous ZrO_2 is dominant in MW-ZrO_2/MWCNTs(C)-8. In contrast, the crystalline zirconia is common in the composite of CH-ZrO_2/MWCNTs(C)-720 from the conventional hydrothermal synthesis.

The residual mass of CH-ZrO_2/MWCNTs(C)-720 after TGA (at 900 °C) is about 36%, which is almost 2.5 times higher than that of MW-ZrO_2/MWCNTs(C)-8 (~13%), indicating that the loading amount of

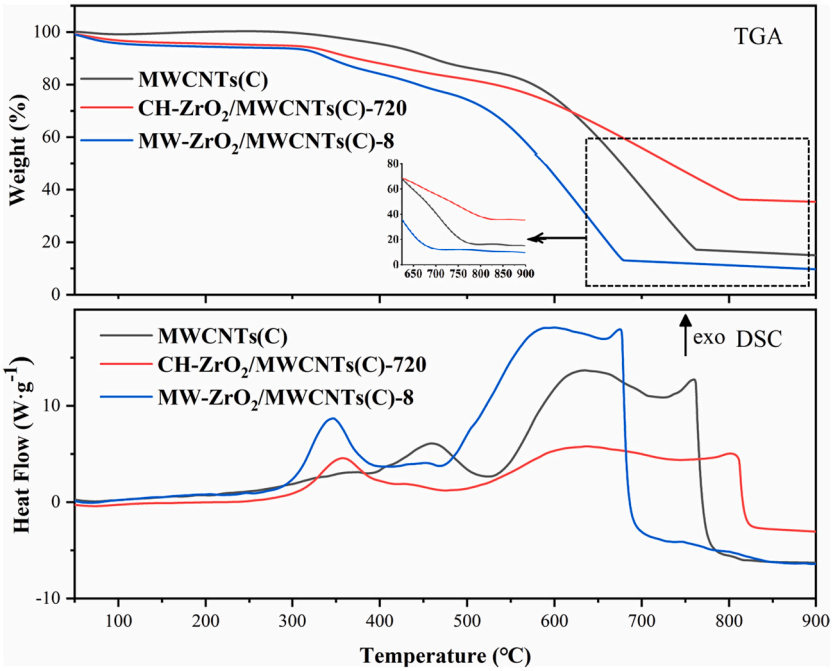

Fig. 4. TGA and DSC analysis of MWCNTs(C), MW-ZrO_2/MWCNTs(C)-8 and CH-ZrO_2/MWCNTs(C)-720.

ZrO_2 in CH-ZrO_2/MWCNTs(C)-720 is much more than that of in MW-ZrO_2/MWCNTs(C)-8. The findings by TGA and DSC agree well with the results of TEM and XRD, which support the discussion on the crystalline structure of the composites prepared by different synthesis methods.

Pyridine FT-IR spectroscopy was used to characterize the nature and amount of acid sites on the composite surface, as shown in Fig. S7 and Table 1. The absorption peaks locatedd at around 1451, 1490 and 1610 cm^{-1} can be assigned to Lewis acid sites, and the absorption peak located at 1540 cm^{-1} is attributed to Brønsted acid sites [45]. Based on the methods reported previously [51,52], surface concentrations of Lewis and Brønsted acid sites were calculated as shown in Table 1, showing that CH-ZrO_2/MWCNTs(C)-720 possesses more surface acidic sites than MW-ZrO_2/MWCNTs(C)-8. While the number of acidic sites of the bulk MW-ZrO_2-8 is between them.

ICP-OES measured the actual Zr content in the three materials of MW-ZrO_2-8, CH-ZrO_2/MWCNTs(C)-720, and MW-ZrO_2/MWCNTs(C)-8 (expressed as Zr wt%), and the results are presented in Table 1. Based on measured data, the bulk MW-ZrO_2-8, the atomic ratio of Zr to O is close to 1:2, indicating that it basically contains no impurities. CH-ZrO_2/MWCNTs(C)-720 prepared by the conventional hydrothermal synthesis possesses higher ZrO_2 loading than MW-ZrO_2/MWCNTs(C)-8. Accordingly, the relatively low acidity of MW-ZrO_2/MWCNTs(C)-8 can be explained by the comparatively low Zr loading on MWCNTs(C) in comparison with that of CH-ZrO_2/MWCNTs(C)-720.

Textural properties of the MWCNTs(C) support and the CH-ZrO_2/MWCNTs(C)-720 and MW-ZrO_2/MWCNTs(C)-8 composite were assessed using N_2 physisorption, and the results are shown in Fig. S8. Nitrogen porosimetry revealed that MWCNTs(C) and the composite based it has the isotherms similar to the type II one, which is basically non-porous, as evidenced by the insignificant rise in the amount adsorbed at low relative pressures. The specific Brunauer-Emmett-Teller (BET) surface area and total pore volume (at $P/P_0 = 0.99$) of the pristine MWCNTs(C) support were measured as 416 $m^2 \cdot g^{-1}$ and 1.79 $cm^3 \cdot g^{-1}$, respectively, which was likely due to the packing of the internal space of MWCNTs(C). After the loading of ZrO_2, the BET surface area, as well as the pore volume of the CH-ZrO_2/MWCNTs(C)-720 and MW-ZrO_2/MWCNTs(C)-8 catalysts, dropped significantly, which could be the result of channel blockage and/or surface coverage (of MWCNTs(C)) caused by the low surface area ZrO_2 phase [53]. In addition, CH-ZrO_2/MWCNTs(C)-720 presented a smaller BET surface area of 164 $m^2 \cdot g^{-1}$ and a lower pore volume of 0.70 $cm^3 \cdot g^{-1}$ in comparison with that of MW-ZrO_2/MWCNTs(C) (192 $m^2 \cdot g^{-1}$ and 0.74 $cm^3 \cdot g^{-1}$, respectively), which suggests that MW-ZrO_2/MWCNTs(C)-8 has a lower zirconia loading.

3.2. *Mechanisms of ZrO_2 deposition on MWCNTs(C)*

Based on the above characterization measurements, highly dispersed amorphous ZrO_2 was successfully deposited on the surface of MWCNTs (C) after the MW synthesis (8 min). Conversely, large crystalline ZrO_2 particles were synthesized on MWCNTs(C) via the time-consuming conventional hydrothermal route (720 min). In order to explain the difference in the ZrO_2 phases resulting from the two synthesis methods, the following mechanisms were proposed, as shown in Fig. 5.

According to previous research [20,54], the reaction paths can be described as Eq. (1) and Eq. (2) that the hydrolysis of $ZrOCl_2$ occurs in an aqueous system, which forms $Zr(OH)_4$ and HCl. With the increase of system temperature, the volatilization of HCl breaks the reaction equilibrium of Eq. (1), leading to the increase of the concentration of Zr $(OH)_4$ that is adsorbed by the MWCNTs(C). Condensation of the adsorbed $Zr(OH)_4$ leads to the formation of the supported ZrO_2 on MWCNTs (C).

Table 1
Acidic properties and Zr content of MW-ZrO_2-8, CH-ZrO_2/MWCNTs(C)-720 and MW-ZrO_2/MWCNTs(C)-8.

Sample	Total acidity (μmol·g^{-1})	Brønsted acid amount (μmol·g^{-1})	Lewis acid amount (μmol·g^{-1})	Brønsted/Lewis	Zr content (%)
CH-ZrO_2/MWCNTs(C)-720	61.91	5.44	56.07	0.096	42.79
MW-ZrO_2/MWCNTs(C)-8	47.09	3.04	44.04	0.069	6.31
MW-ZrO_2-8	85.22	2.98	82.24	0.036	73.32

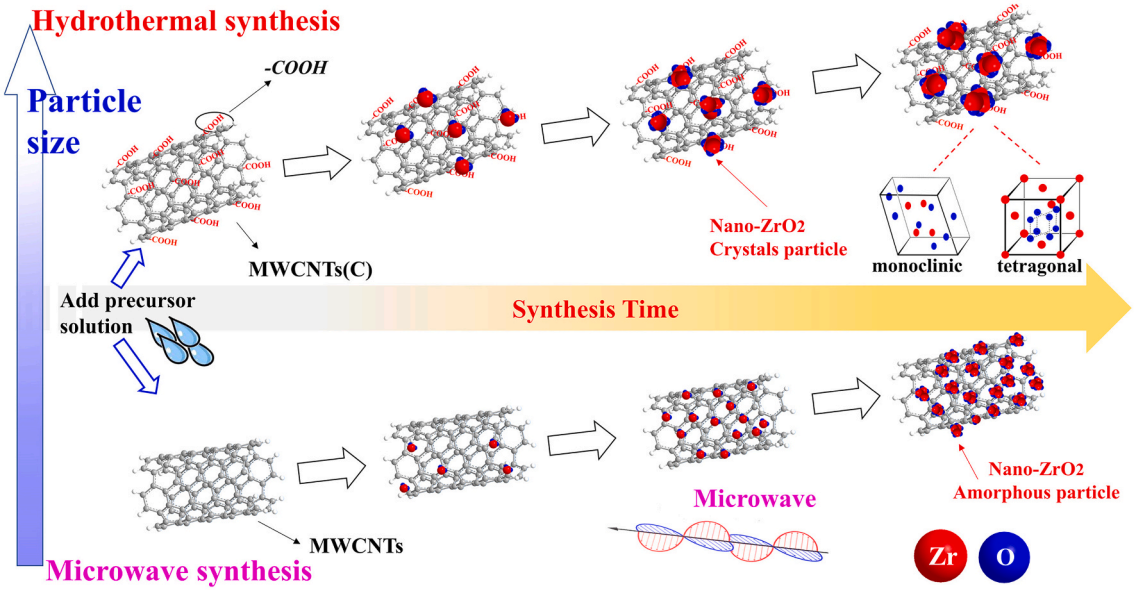

Fig. 5. Proposed growth mechanism of ZrO_2 on MWCNTs in different synthesis routes.

$$ZrOCl_2 + 3H_2O \rightarrow Zr(OH)_4 + 2HCl \quad (1)$$

$$Zr(OH)_4 \rightarrow ZrO_2 + 2H_2O \quad (2)$$

When $Zr(OH)_4$ is formed in the liquid bulk, it tends to interact with the surface carboxyl group via electrostatic adsorption [54]. Accordingly, the past study employing MWCNTs requires the pretreatment of the carbon support (via oxidation) to generate sufficient functional groups on the surface of MWCNTs as nucleation sites to facilitate ZrO_2 growth (via $Zr(OH)_4$ condensation) under hydrostatic conditions [54]. $ZrOCl_2$ could interact with surface —COOH directly via esterification to form the C—O—Zr bond on the surface of MWCNTs and subsequently form ZrO_2 under the conventional hydrothermal synthesis [14,20]. Nevertheless, under the conventional hydrothermal conditions, the presence of O-containing surface groups on MWCNTs is key to the deposition of ZrO_2. As a result, an increase in the size of the deposited ZrO_2 can be expected by extending the synthesis time in these conventional syntheses. In hydrothermal synthesis, the crystalline property of the deposited ZrO_2 is mainly related to the pH value and reaction temperature of the system. Gao et al. showed that high temperatures (150 °C) and acidic conditions (pH <3) could promote the formation of tetragonal ZrO_2 on MWCNTs [20]. Conversely, the monoclinic zirconia nanoparticles supported on MWCNTs were synthesized under low-temperature conditions. Compared to monoclinic ZrO_2, tetragonal ZrO_2 benefits the catalytic properties due to a relatively strong acidity [55,56]. Therefore, the growth mechanism of the supported ZrO_2 on MWCNTs(C) (i.e., CH-ZrO_2/MWCNTs(C)-720) under the hydrothermal condition is well supported by previous studies, which includes the nucleation of Zr precursors on the surface -COOH, followed by the formation of crystalline monoclinic/tetragonal phases on MWCNTs(C), as shown by the mechanism above in Fig. 5. Since the condition used in this work was 180 °C, the tetragonal phase was encouraged in CH-ZrO_2/MWCNTs(C)-720.

Under the MW condition, the rapid and selective heating of the MW absorbing carbon support (i.e. MWCNTs(C)) leads to quite different growth mechanisms of ZrO_2 on MWCNTs(C) from that under the conventional hydrothermal condition [46,57,58]. According to the theory of dielectric heating [49], the higher the dielectric constant and dielectric loss is, the higher the MW absorbing ability of the material is. Especially, MWCNTs(C) have a strong dielectric constant and dielectric loss than surrounding solvents (seen in Table S1), suggesting that the MWCNTs(C) would be selectively and rapidly heated under MW irradiation and generated microscopic "hot spots" over their surface [28]. Such a considerable temperature gradient makes it easier for Zr $(OH)_4$ in solution to undergo decomposition reaction on the superheated MWCNTs(C) surface to form ZrO_2 and uniformly deposit on the MWCNTs(C) surface [40]. While in the conventional hydrothermal synthesis, the MWCNTs(C) support and solution have the same temperature, and $Zr(OH)_4$ is more inclined to decompose in solution [54,59]. Therefore, different from MW hydrothermal synthesis, the surface carboxyl groups of MWCNTs are necessary to provide nucleation sites for the growth of ZrO_2 on the MWCNTS surface in conventional hydrothermal synthesis. In addition, it was also reported that MW irradiation could promote the nucleation and crystallization process of metal oxides such as Silicalite-1 and VSB-5 molecular sieves, and the effect appears to be much more apparent on the nucleation step relative to crystal growth [60].

Consequently, the deposition of ZrO_2 on the MWCNTs(C) under microwave irradiation would not depend on the surface carboxyl groups. With the strong MW-absorbing MWCNTs(C), ZrO_2 was directly deposited on its surface due to the local hot surface under MW irradiation. Since converting the Zr precursor to ZrO_2 is rather quick, the formed ZrO_2 is amorphous rather than crystalline (as evidenced by XRD and TEM analysis above). A similar phenomenon of forming smaller particles and the amorphous phase of bulk ZrO_2 under MW irradiation was also reported previously [40], while the formation of local "hot spots" on MW-absorbing materials under MW irradiation was directly observed in the previous study [28].

Based on the above analysis, the synthesized catalyst was almost inactive without the carboxyl group on the MWCNTs in the conventional hydrothermal synthesis. With the surface groups in the case of MWCNTs (C), ZrO_2 gradually grew into aggregates at the nucleation sites (of carboxyl groups) with an increase in synthesis time, as proposed in Fig. 5. In the MW method, unlike the conventional hydrothermal method, the nucleation of ZrO_2 on the MWCNTs(C) surface under MW irradiation could be no longer dependent on the adsorption sites of carboxyl groups on the support, i.e., direct deposition of ZrO_2 phase on MWCNTs(C) in the MW synthesis was likely.

In summary, in the conventional hydrothermal synthesis, ZrO_2 growth was preferred with the surface —COOH and gradually formed large ZrO_2 particles on MWCNTs(C) with an extended synthesis time, which was also reported previously [60]. However, the aggregation of the ZrO_2 phase on MWCNTs(C) reduces the availability of the relevant

reactive sites on the carbon support, resulting in a relatively low catalyst activity (to be discussed later). Conversely, in the MW synthesis, the strong absorption of MW by MWCNTs(C) creates local "hot spots" on their surface, which enable the formation of highly dispersed and small ZrO_2 particles to increase the effective contact area between the reactants and the catalyst [14,30]. In addition, the amorphous structure could be more beneficial in the catalytic conversion of fructose than the monoclinic and tetragonal phases [49], which will be discussed below.

3.3. Catalytic conversion of fructose to 5-HMF over the composite catalysts

The developed ZrO_2/MWCNTs(C) composite catalysts and the control catalysts were assessed in the model reaction of catalytic fructose conversion to 5-HMF to investigate their activity. Under the same catalytic condition (i.e., 0.5 g fructose with 0.2 g catalyst under 20 mL DMSO at 120 °C bulk system temperature and atmospheric pressure), the catalytic performance of the MW-ZrO_2-8 (bulk), MW-ZrO_2/MWCNTs(C)-8 and CH-ZrO_2/MWCNTs(C)-720 catalyst were obtained and presented in Fig. 6. It was found that, under the reaction condition used, dehydration of fructose could proceed over all the catalysts. Comparatively, the CH-ZrO_2/MWCNTs(C)-8 catalyst was the least active one compared to the MW-ZrO_2/MWCNTs(C)-8 and bulk MW-ZrO_2-8. In detail, a fructose conversion of 24.8% and a 5-HMF yield of 15.7% were achieved by CH-ZrO_2/MWCNTs(C)-720 after a 5-min reaction. While MW-ZrO_2/MWCNTs(C)-8 achieved 72.8% and 63.0, and the bulk MW-ZrO_2-8 achieved 53.25% and 41.27%, respectively. For the reaction catalyzed over CH-ZrO_2/MWCNTs(C)-720 and MW-ZrO_2-8, the catalytic system could reach the steady-state after 60 min on stream. Conversely, over MW-ZrO_2/MWCNTs(C)-8, steady-state was quickly established in 20 min, leading to a 5-HMF yield of 86.1%, which suggests that MW-ZrO_2/MWCNTs(C)-8 can improve the reaction kinetics significantly in comparison with CH-ZrO_2/MWCNTs(C)-720. As shown in Table S2, carbon balance of the catalytic reactions are above 92%.

The effect of the bulk system temperature and catalyst loading on the performance of MW-ZrO_2/MWCNT(C)-8 for catalyzing fructose conversion was studied, and the results were shown in Fig. S9. The bulk system temperature affected fructose conversion and 5-HMF yield positively. In the presence of the MW-ZrO_2/MWCNT(C)-8 catalyst, fructose conversion increased with an increase in catalyst amount, with the maximum 5-HMF yield of about 63% in the case of 0.2 g MW-ZrO_2/MWCNT(C)-8 with 0.5 g fructose (i.e., 40 wt%). However, a further increase of the catalyst loading from 40 wt% caused the decrease in 5-HMF yield due to the production of by-products, as evidenced by Fig. S10 and Table S3.

The acidity of the catalyst could play a vital role, especially in the catalytic conversion of sugars into 5-HMF, and Brønsted acid sites promoted the dehydration of fructose to form HMF [61]. Turnover frequency (TOF) was calculated from the rate of produced 5-HMF (5 min) and acid site concentration (Brønsted acid sites) [62], as listed in Table 2. This reaction rate of MW-ZrO_2/MWCNTs(C)-8 was nearly four times that of CH-ZrO_2/MWCNTs(C)-720, and the TOF of MW-ZrO_2/MWCNTs(C)-8 was more than seven times that of CH-ZrO_2/MWCNTs(C)-720. MW-ZrO_2/MWCNTs(C)-8 showed the highest catalytic activity despite the low acidity, indicating that the amorphous ZrO_2 structure enhanced the reaction rate. According to the catalytic and characterization data of the catalysts, the particle size and degree of aggregation of the supported ZrO_2 could be important factors to affect the catalytic activity in the selective conversion of fructose to 5-HMF. Regarding CH-ZrO_2/MWCNTs(C)-720, although its crystallinity and acidity are high

Table 2
Catalytic activity of MW-ZrO_2-8, CH-ZrO_2/MWCNTs(C)-720 and MW-ZrO_2/MWCNTs(C)-8.

Sample	Rate of 5-HMF production[a] ($mmol \cdot L^{-1} \cdot min^{-1}$)	TOF[b] (min^{-1})
CH-ZrO_2/MWCNTs(C)-720	4.7	80.1
MW-ZrO_2/MWCNTs(C)-8	17.5	574.9
MW-ZrO_2-8	11.5	384.4

[a] Reaction conditions: 0.5 g fructose, 0.2 g catalyst, 20 mL DMSO, at 120 °C and atmospheric pressure for 5 min.
[b] TOF was estimated from the initial rate per Brønsted acid sites [62].

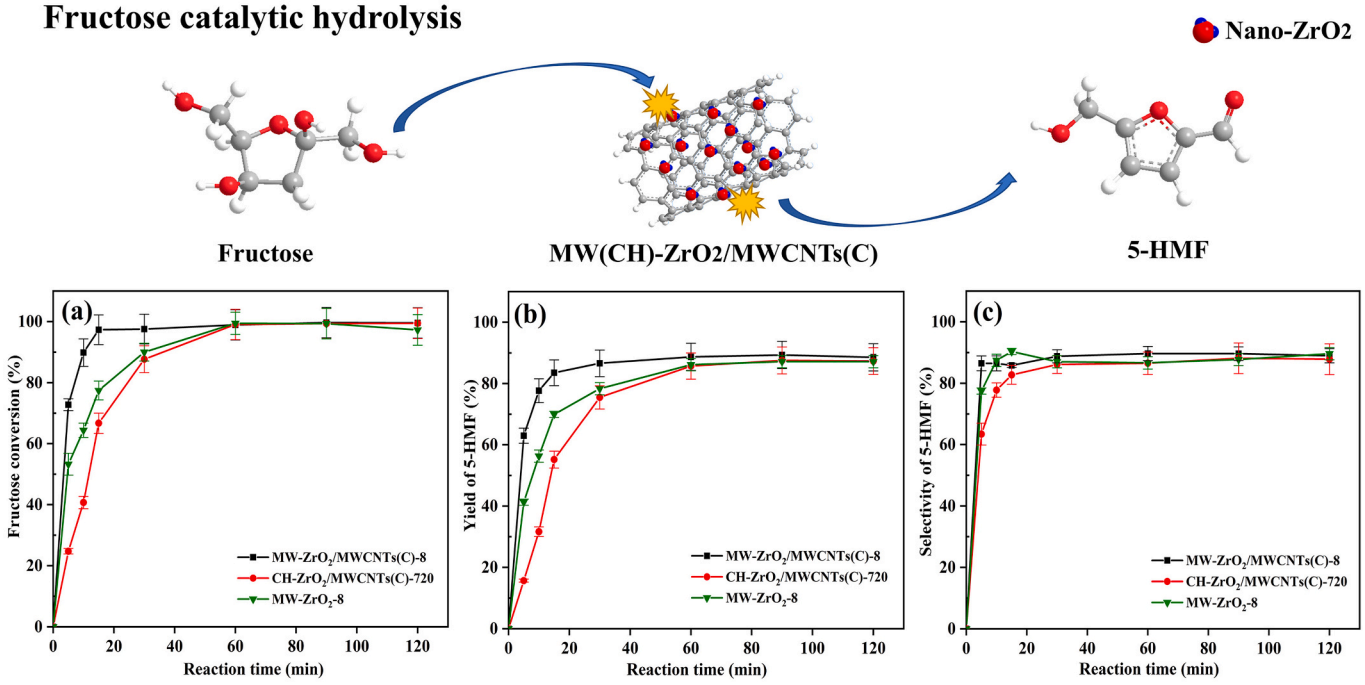

Fig. 6. (a) Fructose conversion, (b) selectivity to 5-HMF and (c) 5-HMF yield over the catalysts under investigation. Reaction conditions: 0.5 g fructose, 0.2 g catalyst, 20 mL DMSO, at 120 °C and atmospheric pressure.

(compared to that of MW-ZrO_2/MWCNTs(C)-8), its catalytic activity was relatively poor, which could be due to severe aggregation of the deposited ZrO_2 on MWCNTs(C), limiting the available active sites for catalysis. Conversely, for MW-ZrO_2/MWCNTs(C)-8, the highly dispersed amorphous ZrO_2 with smaller particle sizes showed a better catalytic activity, suggesting that crystallinity might not be the key for explaining the catalytic activity of the supported in ZrO_2 catalysis.

In order to assess the performance of the developed MW-ZrO_2/MWCNTs(C)-8 catalyst, a comparison with state of the art regarding fructose dehydration and 5-HMF yield was carried out (Table S4 and Table S5). Compared to the studies employing metal oxides, zeolites, ion exchange resin and sulfonated carbons, the MW-ZrO_2/MWCNTs(C)-8 catalyst shows excellent catalytic activity in catalytic fructose conversion, whilst showing the performance of CH-ZrO_2/MWCNTs(C)-720 is relatively low. Hence, the advantage of the highly dispersed amorphous ZrO_2 the MW-ZrO_2/MWCNTs(C)-8 catalyst, which was synthesized by the efficient MW synthesis, is highlighted.

Regarding the recyclability of MW-ZrO_2/MWCNTs(C)-8 and CH-ZrO_2/MWCNTs(C)-720, experimental results (Fig. S11) show that both of them has good cycling stability. 5-HMF yield over CH-ZrO_2/MWCNTs (C)-720 decreased with an increase in the number of stability cycles, and the difference in the 5-HMF yield for the initial and final cycle was approximately 5%. Deactivation of MW-ZrO_2/MWCNTs(C)-8 was also measured, regarding 5-HMF yield over MW-ZrO_2/MWCNTs(C)-8, it dropped by ~12.5% (from 62.9% to 50.4%) at the end of the stability test. Deactivation of the composite catalysts might be due to the coke deposition on the active sites and/or leaching of the ZrO_2 nanoparticles, as shown in Table S6 and Fig. S7. However, TEM analysis of the used catalysts (after 5 recycles, Fig. S12) showed no apparent changes of size and original superstructure in comparison with the fresh ones, indicating a stable catalyst structure.

Additionally, it was also found that under the MW condition, the particle size of the supported ZrO_2 could be increased by prolonging the synthesis time, as shown in Fig. S13. However, the increase in ZrO_2 particle sizes was not beneficial to the 5-HMF yield in fructose conversion. At the same time, it was also found that during the MW synthesis surface -COOH group was not the prerequisite for enabling the growth of ZrO_2. Conversely, the dielectric constant and dielectric loss of the carbon supports played a role in the process, as shown in Table S1, which affected their catalytic efficiency in the selective conversion of fructose to 5-HMF. Experiment for higher initial zirconia concentration was also carried out and it was found that microwave synthesis still demonstrated superior performance (Fig. S14).

4. Conclusions and perspectives

This work presents the preparation of ZrO_2 supported on MWCNTs (C) composite using an efficient microwave (MW) synthesis method for converting fructose to 5-HMF effectively and efficiently. Based on the comparative characterization of ZrO_2/MWCNTs(C) composites prepared by the conventional hydrothermal and the developed MW-assisted synthesis methods, the physiochemical properties of the MW-synthesized ZrO_2/MWCNTs(C) composite (i.e., MW-ZrO_2/MWCNTs (C)-8) were revealed. In detail, highly dispersed amorphous ZrO_2 with very small particle sizes (about 4.5 nm) was found in MW-ZrO_2/MWCNTs(C)-8. Conversely, the conventional method promoted the large aggregation of crystalline ZrO_2 on MWCNTs(C) (i.e. in CH-ZrO_2/MWCNTs(C)-720). Such difference was attributed to the selective and rapid heating of the strong MW-absorbing support of MWCNTs(C) under MW irradiation, leading to the formation of microscopic “hot spots” and therefore resulting in the rapid deposition of amorphous ZrO_2 nanoparticles on the surface of MWCNTs(C). More importantly, the developed MW method did not depend on surface carboxyl groups of the carbon support, while carboxyl groups were demanded under the conventional hydrothermal condition for nucleation of Zr species for crystal growth.

The composite materials under investigation were assessed in catalytic fructose conversion (to 5-HMF). MW-ZrO_2/MWCNTs(C)-8 showed a better catalytic performance than that of CH-ZrO_2/MWCNTs(C)-720 (which was prepared by the conventional hydrothermal synthesis) and MW-ZrO_2-8 (the unsupported bulk ZrO_2 prepared by the MW method) regarding fructose conversion and 5-HMF yield For example, MW-ZrO_2/MWCNTs(C)-8 achieved 72.8% fructose conversion and 63.0% 5-HMF yield in 5 min, whilst CH-ZrO_2/MWCNTs(C)-720 only obtained 24.8% and 15.7%, respectively. The good catalytic performance of MW-ZrO_2/MWCNTs(C)-8 can be related to its unique amorphous ZrO_2 phase supported on MWCNTs(C). In summary, the findings of the work shed light on the effectiveness of the MW-assisted synthesis, especially in combination with MW-absorbing materials, which can be further explored for other relevant systems requiring process intensification. For example, the employment of MW-responsive catalysts for process intensification of catalytic conversion of biomass and bio-derived chemicals under MW irradiation.

CRediT authorship contribution statement

Shiyun Mu: Conceptualization, Methodology, Formal analysis, Investigation, Writing – original draft. **Kai Liu:** Conceptualization, Methodology, Formal analysis, Investigation, Writing – original draft. **Hong Li:** Writing – review & editing, Project administration. **Zhenyu Zhao:** Methodology, Writing – review & editing. **Xiaoqi Lyu:** Methodology. **Yilai Jiao:** Writing – review & editing, Formal analysis. **Xingang Li:** Resources. **Xin Gao:** Resources, Conceptualization, Formal analysis, Funding acquisition, Writing – review & editing, Supervision. **Xiaolei Fan:** Resources, Writing – review & editing, Formal analysis, Supervision.

Declaration of Competing Interest

The authors declare that they have no known competing financial interests or personal relationships that could have appeared to influence the work reported in this paper.

Acknowledgements

This project has received funding from the European Union’s Horizon 2020 research and innovation programme under grant agreement No 872102. The authors at Tianjin University also acknowledge the financial support from the National Key R&D Program of China (No. 2019YFE0123200), the National Natural Science Foundation of China (No. 22078348) and Haihe Laboratory of Sustainable Chemical Transformations.

Appendix A. Supplementary data

Supplementary data to this article can be found online at https://doi.org/10.1016/j.fuproc.2022.107292.

References

[1] Y.X. Jing, Y. Guo, Q.N. Xia, X.H. Liu, Y.Q. Wang, Catalytic production of value-added chemicals and liquid fuels from lignocellulosic biomass, Chem 5 (10) (2019) 2520–2546, https://doi.org/10.1016/j.chempr.2019.05.022.
[2] C.W.J. Murnaghan, N. Skillen, C. Hardacre, J. Bruce, G.N. Sheldrake, P.K. J. Robertson, Exploring lignin valorisation: the application of photocatalysis for the degradation of the beta-5 linkage, J. Phys. Energy 3 (3) (2021), https://doi.org/10.1088/2515-7655/abf853.
[3] L.T. Mika, E. Csefalvay, A. Nemeth, Catalytic conversion of carbohydrates to initial platform chemicals: chemistry and sustainability, Chem. Rev. 118 (2) (2018) 505–613, https://doi.org/10.1021/acs.chemrev.7b00395.
[4] M. Sameeroddin, M.K.G. Deshmukh, G. Viswa, M.A. Sattar, Renewable energy: fuel from biomass, production of ethanol from various sustainable sources by fermentation process, Materials Today: Proc. (2021), https://doi.org/10.1016/j.matpr.2021.01.746.

[5] S. Nawaz, M. Ahmad, S. Asif, J.J. Klemeš, M. Mubashir, M. Munir, M. Zafar, A. Bokhari, A. Mukhtar, S. Saqib, K.S. Khoo, P.L. Show, Phyllosilicate derived catalysts for efficient conversion of lignocellulosic derived biomass to biodiesel: a review, Bioresour. Technol. 343 (2022), 126068, https://doi.org/10.1016/j.biortech.2021.126068.

[6] M. Govarthanan, S. Manikandan, R. Subbaiya, R.Y. Krishnan, S. Srinivasan, N. Karmegam, W. Kim, Emerging trends and nanotechnology advances for sustainable biogas production from lignocellulosic waste biomass: a critical review, Fuel 312 (2022), 122928, https://doi.org/10.1016/j.fuel.2021.122928.

[7] S. Mardiana, N.J. Azhari, T. Ilmi, G.T.M. Kadja, Hierarchical zeolite for biomass conversion to biofuel: a review, Fuel 309 (2022), https://doi.org/10.1016/j.fuel.2021.122119.

[8] R.D. Prasad, A. Raturi, Prospects of Sustainable Biomass-based Power Generation in a Small Island Country, J. Clean. Prod. 318 (2021), https://doi.org/10.1016/j.jclepro.2021.128519.

[9] R. Mariscal, P. Maireles-Torres, M. Ojeda, I. Sadaba, M.L. Granados, Furfural: a renewable and versatile platform molecule for the synthesis of chemicals and fuels, Energy Environ. Sci. 9 (4) (2016) 1144–1189, https://doi.org/10.1039/c5ee02666k.

[10] V.G. Deshmane, Y.G. Adewuyi, Synthesis of thermally stable, high surface area, nanocrystalline mesoporous tetragonal zirconium dioxide (ZrO2): Effects of different process parameters, Microporous Mesoporous Mater. 148 (1) (2012) 88–100, https://doi.org/10.1016/j.micromeso.2011.07.012.

[11] H. Gao, Y. Huang, X. Zhang, Z.A.S. Bairq, Y. Huang, P. Tontiwachwuthikul, Z. Liang, Catalytic performance and mechanism of SO42−/ZrO2/SBA-15 catalyst for CO2 desorption in CO2-loaded monoethanolamine solution, Appl. Energy 259 (2020), https://doi.org/10.1016/j.apenergy.2019.114179.

[12] H. Zhou, J.M. Saad, Q. Li, Y. Xu, Steam reforming of polystyrene at a low temperature for high H2/CO gas with bimetallic Ni-Fe/ZrO2 catalyst, Waste Manag. 104 (2020) 42–50, https://doi.org/10.1016/j.wasman.2020.01.017.

[13] T.B. Medvedeva, O.L. Ogorodnikova, I.S. Yakovleva, L.A. Isupova, O.P. Taran, N. V. Gromov, V.N. Parmon, Impact of Design on the activity of ZrO2 catalysts in cellulose hydrolysis-dehydration to glucose and 5-hydroxymethylfurfural, Catalysts 11 (11) (2021), https://doi.org/10.3390/catal11111359.

[14] C. Liu, S. Lee, D. Su, B. Lee, S. Lee, R.E. Winans, C. Yin, S. Vajda, L. Pfefferle, G. L. Haller, Controlling the particle size of ZrO2 nanoparticles in hydrothermally stable ZrO2/MWCNT composites, Langmuir 28 (49) (2012) 17159–17167, https://doi.org/10.1021/la303545y.

[15] S. Buinachev, M.A. Mashkovtsev, N. Zhirenkina, D. Aleshin, A. Dankova, A new approach for the synthesis of monodisperse zirconia powders with controlled particle size, Int. J. Hydrog. Energy 46 (32) (2021) 16878–16887, https://doi.org/10.1016/j.ijhydene.2021.01.134.

[16] S.J. Roberts, J.J. Dodson, P.L. Carpinone, H.E. Hagelin-Weaver, Evaluation of nanoparticle zirconia supports in the thermochemical water splitting cycle over iron oxides, Int. J. Hydrog. Energy 40 (46) (2015) 15972–15984, https://doi.org/10.1016/j.ijhydene.2015.09.109.

[17] L. Li, B. Yan, H. Li, S. Yu, X. Ge, Decreasing the acid value of pyrolysis oil via esterification using ZrO2/SBA-15 as a solid acid catalyst, Renew. Energy 146 (2020) 643–650, https://doi.org/10.1016/j.renene.2019.07.015.

[18] Y. Ai, L. Liu, K. Jing, L. Qi, Z. Fan, J. Zhou, H.-B. Sun, Z. Shao, Q. Liang, Noncovalently functionalized carbon nanotubes immobilized Fe–Bi bimetallic oxides as a heterogeneous nanocatalyst for reduction of nitroaromatics, Nano-Structures Nano-Objects 10 (2017) 116–124, https://doi.org/10.1016/j.nanoso.2017.03.012.

[19] N. Wu, X. Ji, L. Li, J. Zhu, X. Lu, Mesoscience in supported nano-metal catalysts based on molecular thermodynamic modeling: a mini review and perspective, Chem. Eng. Sci. 229 (2021), https://doi.org/10.1016/j.ces.2020.116164.

[20] Y. Shan, L. Gao, Synthesis and characterization of phase controllable ZrO2–carbon nanotube nanocomposites, Nanotechnology 16 (6) (2005) 625–630, https://doi.org/10.1088/0957-4484/16/6/001.

[21] K. Pal, D.J. Kang, J.K. Kim, Microstructural investigations of zirconium oxide—on core–shell structure of carbon nanotubes, J. Nanopart. Res. 13 (6) (2010) 2597–2607, https://doi.org/10.1007/s11051-010-0152-7.

[22] J. Lu, J.B. Zang, S.X. Shan, H. Huang, Y.H. Wang, Synthesis and characterization of core-shell structural MWNT-zirconia nanocomposites, Nano Lett. 8 (11) (2008) 4070–4074, https://doi.org/10.1021/nl801841r.

[23] Z. Cheng, H. Lyu, B. Shen, J. Tian, Y. Sun, C. Wu, Removal of antimonite (Sb(III)) from aqueous solution using a magnetic iron-modified carbon nanotubes (CNTs) composite: Experimental observations and governing mechanisms, Chemosphere 288 (Pt 2) (2022), 132581, https://doi.org/10.1016/j.chemosphere.2021.132581.

[24] C. Liu, S. Lee, D. Su, Z. Zhang, L. Pfefferle, G.L. Haller, Synthesis and characterization of nanocomposites with strong interfacial interaction: sulfated ZrO2 nanoparticles supported on multiwalled carbon nanotubes, J. Phys. Chem. C 116 (41) (2012) 21742–21752, https://doi.org/10.1021/jp302377p.

[25] Z. Zhao, H. Li, K. Zhao, L. Wang, X. Gao, Microwave-assisted synthesis of MOFs: rational design via numerical simulation, Chem. Eng. J. 428 (2022), https://doi.org/10.1016/j.cej.2021.131006.

[26] Q. Yi, J. Lan, J. Ye, H. Zhu, Y. Yang, Y. Wu, K. Huang, A simulation method of coupled model for a microwave heating process with multiple moving elements, Chem. Eng. Sci. 231 (2021), https://doi.org/10.1016/j.ces.2020.116339.

[27] Z. Zhao, H. Li, K. Zhao, L. Wang, X. Gao, Microwave-assisted synthesis of MOFs: rational design via numerical simulation, Chem. Eng. J. 428 (2022), 131006, https://doi.org/10.1016/j.cej.2021.131006.

[28] Z. Zhao, X. Shen, H. Li, K. Liu, H. Wu, X. Li, X. Gao, Watching microwave-induced microscopic hot spots via the thermosensitive fluorescence of Eu/Tb mixed metal organic complexes, Angew. Chem. Int. Ed. Eng. 61 (6) (2022), e202114340, https://doi.org/10.1002/anie.202114340.

[29] X. Ou, S. Xu, J.M. Warnett, S.M. Holmes, A. Zaheer, A.A. Garforth, M.A. Williams, Y. Jiao, X. Fan, Creating hierarchies promptly: Microwave-accelerated synthesis of ZSM-5 zeolites on macrocellular silicon carbide (SiC) foams, Chem. Eng. J. 312 (2017) 1–9, https://doi.org/10.1016/j.cej.2016.11.116.

[30] T. Ji, R. Tu, L. Mu, X. Lu, J. Zhu, Structurally tuning microwave absorption of core/shell structured CNT/polyaniline catalysts for energy efficient saccharide-HMF conversion, Appl. Catal. B Environ. 220 (2018) 581–588, https://doi.org/10.1016/j.apcatb.2017.08.066.

[31] X. Lyu, H. Li, H. Xiang, Y. Mu, N. Ji, X. Lu, X. Fan, X. Gao, Energy efficient production of 5-hydroxymethylfurfural (5-HMF) over surface functionalized carbon superstructures under microwave irradiation, Chem. Eng. J. 428 (2022), https://doi.org/10.1016/j.cej.2021.131143.

[32] A. Meng, L. Lin, X. Yuan, T. Shen, Z. Li, Q. Li, Ag/ZrO2/MWCNT nanocomposite as non-platinum electrocatalysts for enhanced oxygen reduction reaction, Chemcatchem 11 (12) (2019) 2900–2908, https://doi.org/10.1002/cctc.201900317.

[33] S.K. Lau, D. Dag, S. Ozturk, F. Kong, J. Subbiah, A comparison between the open-ended coaxial probe method and the parallel plate method for measuring the dielectric properties of low-moisture foods, Lwt 130 (2020), https://doi.org/10.1016/j.lwt.2020.109719.

[34] F. Lupo, R. Kamalakaran, C. Scheu, N. Grobert, M. Ruhle, Microstructural investigations on zirconium oxide-carbon nanotube composites synthesized by hydrothermal crystallization, Carbon 42 (10) (2004) 1995–1999, https://doi.org/10.1016/j.carbon.2004.03.037.

[35] M. Romero-Saez, A.B. Dongil, N. Benito, R. Espinoza-Gonzalez, N. Escalona, F. Gracia, CO2 methanation over nickel-ZrO2 catalyst supported on carbon nanotubes: a comparison between two impregnation strategies, Appl. Catal. B-Environ. 237 (2018) 817–825, https://doi.org/10.1016/j.apcatb.2018.06.045.

[36] Y. Quan, N. Zhang, Z. Zhang, Y. Han, J. Zhao, J. Ren, Enhanced performance of Ni catalysts supported on ZrO2 nanosheets for CO2 methanation: Effects of support morphology and chelating ligands, Int. J. Hydrog. Energy 46 (27) (2021) 14395–14406, https://doi.org/10.1016/j.ijhydene.2021.01.236.

[37] Y. Wu, H. Wang, L. Wang, N. Gong, J. Yang, T. Zhang, H. Xie, Y. Tan, Effect of iron on ZrO2-based catalysts for direct synthesis of isobutanol from syngas, Fuel 304 (2021), https://doi.org/10.1016/j.fuel.2021.121342.

[38] N.S. Hassan, A.A. Jalil, S. Triwahyono, N.F. Khusnun, S.M. Izan, K. Kidam, A. Johari, Synergistic effect of microwave rapid heating and weak mineralizer on silica-stabilized tetragonal zirconia nanoparticles for enhanced photoactivity of Bisphenol A, J. Mol. Liq. 261 (2018) 423–430, https://doi.org/10.1016/j.molliq.2018.04.068.

[39] V.B. Raghavendra, S. Naik, M. Antony, G. Ramalingam, M. Rajamathi, S. Raghavan, Amorphous, monoclinic, and tetragonal porous zirconia through a controlled self-sustained combustion route, J. Am. Ceram. Soc. 94 (6) (2011) 1747–1755, https://doi.org/10.1111/j.1551-2916.2010.04334.x.

[40] C. Li, K. Li, H. Li, Y. Zhang, H. Ouyang, L. Liu, C. Sun, Effect of reaction temperature on crystallization of nanocrystalline zirconia synthesized by microwave-hydrothermal process, J. Alloys Compd. 561 (2013) 23–27, https://doi.org/10.1016/j.jallcom.2013.01.157.

[41] V.C. Nguyen, A. Dandach, T.T.H. Vu, P. Fongarland, N. Essayem, ZrW catalyzed cellulose conversion in hydrothermal conditions: Influence of the calcination temperature and insights on the nature of the active phase, Molecular Catalysis 476 (2019), https://doi.org/10.1016/j.mcat.2019.110518.

[42] S.A. Ntim, S. Mitra, Adsorption of arsenic on multiwall carbon nanotube-zirconia nanohybrid for potential drinking water purification, J. Colloid Interface Sci. 375 (2012) 154–159, https://doi.org/10.1016/j.jcis.2012.01.063.

[43] S. Mallik, K.M. Parida, S.S. Dash, Studies on heteropoly acid supported zirconia, J. Mol. Catal. A Chem. 261 (2) (2007) 172–179, https://doi.org/10.1016/j.molcata.2006.07.073.

[44] I. Georgieva, N. Danchova, S. Gutzov, N. Trendafilova, DFT modeling, UV-Vis and IR spectroscopic study of acetylacetone-modified zirconia sol-gel materials, J. Mol. Model. 18 (6) (2012) 2409–2422, https://doi.org/10.1007/s00894-011-1257-3.

[45] G. Wang, G. Zhu, Y. Ding, C. Xia, Z. Li, Mesoporous acidic functional N-containing ZrNxOy material for polyoxymethylene diethyl ethers synthesis under mild conditions, Molecular Catalysis 506 (2021), https://doi.org/10.1016/j.mcat.2021.111541.

[46] J. Tian, Q. Shao, J. Zhao, D. Pan, M. Dong, C. Jia, T. Ding, T. Wu, Z. Guo, Microwave solvothermal carboxymethyl chitosan templated synthesis of TiO2/ZrO2 composites toward enhanced photocatalytic degradation of Rhodamine B, J. Colloid Interface Sci. 541 (2019) 18–29, https://doi.org/10.1016/j.jcis.2019.01.069.

[47] M.K. Dongare, A.M. Dongare, V.B. Tare, E. Kemnitz, Synthesis and characterization of copper-stabilized zirconia as an anode material for SOFC, Solid State Ionics 152-153 (2002) 455–462, https://doi.org/10.1016/S0167-2738(02)00371-5.

[48] W. Cai, Q. Zhong, S. Zhang, J. Zhang, Effects of Cr on the NO oxidation over the ceria–zirconia solid solution, RSC Adv. 3 (19) (2013), https://doi.org/10.1039/c3ra40226f.

[49] A.G. Sato, D.P. Volanti, D.M. Meira, S. Damyanova, E. Longo, J.M.C. Bueno, Effect of the ZrO2 phase on the structure and behavior of supported Cu catalysts for ethanol conversion, J. Catal. 307 (2013) 1–17, https://doi.org/10.1016/j.jcat.2013.06.022.

[50] H. Nayebzadeh, N. Saghatoleslami, M. Tabasizadeh, Application of microwave irradiation for fabrication of sulfated ZrO2–Al2O3 nanocomposite via combustion method for esterification reaction: process condition evaluation, J. Nanostructure Chem. 9 (2) (2019) 141–152, https://doi.org/10.1007/s40097-019-0304-y.

[51] E. Hong, S.W. Baek, M. Shin, Y.W. Suh, C.H. Shin, Effect of aging temperature during refluxing on the textural and surface acidic properties of zirconia catalysts, J. Ind. Eng. Chem. 54 (2017) 137–145, https://doi.org/10.1016/j.jiec.2017.05.026.
[52] C.A. Emeis, Determination of Integrated Molar Extinction Coefficients for infrared Absorption Bands of Pyridine Adsorbed on Solid Acid Catalysts, J. Catal. 141 (2) (1993) 347–354.
[53] J. Mielby, K.H. Møller, D. Iltsiou, F. Goodarzi, K. Enemark-Rasmussen, S. Kegnæs, A shortcut to high-quality gmelinite through steam-assisted interzeolite transformation, Microporous Mesoporous Mater. 330 (2022), https://doi.org/10.1016/j.micromeso.2021.111606.
[54] J. Lu, J.B. Zang, S.X. Shan, H. Huang, Y.H. Wang, Synthesis and Characterization of Core−Shell Structural MWNT−Zirconia Nanocomposites, Nano Lett. 8 (11) (2008) 4070–4074, https://doi.org/10.1021/nl801841r.
[55] W. Zhang, Y. Zhu, H. Xu, M. Gaborieau, J. Huang, Y. Jiang, Glucose conversion to 5-hydroxymethylfurfural on zirconia: Tuning surface sites by calcination temperatures, Catal. Today 351 (2020) 133–140, https://doi.org/10.1016/j.cattod.2018.10.002.
[56] I.J. Kuo, N. Suzuki, Y. Yamauchi, K.C.W. Wu, Cellulose-to-HMF conversion using crystalline mesoporous titania and zirconia nanocatalysts in ionic liquid systems, RSC Adv. 3 (6) (2013) 2028–2034, https://doi.org/10.1039/c2ra21805d.
[57] Y. Zheng, Y. Tian, S. Liu, X. Tan, S. Wang, Q. Guo, J. Luo, Z. Li, One-step microwave synthesis of NiO/NiS@CNT nanocomposites for high-cycling-stability supercapacitors, J. Alloys Compd. 806 (2019) 170–179, https://doi.org/10.1016/j.jallcom.2019.07.213.
[58] J.A. Gerbec, D. Magana, A. Washington, G.F. Strouse, Microwave-enhanced reaction rates for nanoparticle synthesis, J. Am. Chem. Soc. 127 (45) (2005) 15791–15800, https://doi.org/10.1021/ja052463g.
[59] Y. Ou, W.-C. Tsen, S.-C. Jang, F.-S. Chuang, J. Wang, H. Liu, S. Wen, C. Gong, Novel composite polymer electrolyte membrane using solid superacidic sulfated zirconia - Functionalized carbon nanotube modified chitosan, Electrochim. Acta 264 (2018) 251–259, https://doi.org/10.1016/j.electacta.2018.01.131.
[60] S.H. Jhung, T. Jin, Y.K. Hwang, J.-S. Chang, Microwave effect in the fast synthesis of microporous materials: which stage between nucleation and crystal growth is accelerated by microwave irradiation? Chem. Eur. J. 13 (16) (2007) 4410–4417, https://doi.org/10.1002/chem.200700098.
[61] J. Guo, S. Zhu, Y. Cen, Z. Qin, J. Wang, W. Fan, Ordered mesoporous Nb–W oxides for the conversion of glucose to fructose, mannose and 5-hydroxymethylfurfural, Appl. Catal. B Environ. 200 (2017) 611–619, https://doi.org/10.1016/j.apcatb.2016.07.051.
[62] C. Tagusagawa, A. Takagaki, A. Iguchi, K. Takanabe, J.N. Kondo, K. Ebitani, T. Tatsumi, K. Domen, Synthesis and characterization of mesoporous Ta−W oxides as strong solid acid catalysts, Chem. Mater. 22 (10) (2010) 3072–3078, https://doi.org/10.1021/cm903767n.